

## Diffusion mechanisms in Cu grain boundaries

Mads R. Sørensen

*Theoretical Division, Los Alamos National Laboratory, Los Alamos, New Mexico 87545*

Yuri Mishin

*Department of Materials Science and Engineering, Virginia Polytechnic Institute and State University, Blacksburg, Virginia 24061-0237*

Arthur F. Voter

*Theoretical Division, Los Alamos National Laboratory, Los Alamos, New Mexico 87545*

(Received 7 April 2000)

We investigate atomic mechanisms of grain boundary (GB) diffusion by combining molecular dynamics (MD), molecular statics, the harmonic approximation to atomic vibrations, and kinetic Monte Carlo (KMC) simulations. The most important aspects of this approach are the basin-constrained implementation of MD and an automated location of transition states using the nudged elastic band method. We study two  $\Sigma=5$  [001] symmetric tilt GB's in Cu, with atomic interactions described by an embedded-atom potential. Our simulations demonstrate that GB's support both vacancies and interstitials, and that vacancies can show interesting effects such as delocalization and instability at certain GB sites. Besides simple vacancy-atom exchanges, vacancies move by "long jumps" involving a concerted motion of two atoms. Interstitials move through concerted displacements of two or more atoms. More complex mechanisms (such as ring processes) involving larger groups of atoms have also been found. The obtained point defect formation energies and entropies, as well as their migration rate constants calculated within harmonic transition state theory, are used as input to KMC simulations of GB diffusion. The simulations show that GB diffusion can be dominated by either vacancy or interstitial-related mechanisms depending on the GB structure. The KMC simulations also reveal interesting effects such as temperature-dependent correlation factors and the trapping effect. Using the same simulation approach we study mechanisms of point defect generation in GB's and show that such mechanisms also involve collective transitions.

### I. INTRODUCTION

Grain boundaries (GB's) are known to provide easy paths for mass transport in materials since the energies of defect formation and migration in GB's tend to be lower than in the bulk lattice. GB diffusion is a technologically important topic. Kinetics of many microstructural changes, phase transformations, and solid-state reactions in engineering materials are often controlled by GB diffusion.<sup>1</sup> Moreover, migration and accumulation of point defects in GB's can lead to void formation, which can cause materials degradation and failure. For a recent review in the area see Ref. 2.

Traditionally, atomistic simulation studies of GB diffusion have followed two separate lines: they have employed either molecular dynamics (MD) (Refs. 3–7) or static calculations combined with kinetic Monte Carlo (KMC) simulations.<sup>8–12</sup> The advantage of MD is that the equations of motion of the atoms are solved directly and all atomic transitions that can happen in a real system can also happen in the simulation, at least in principle. A shortcoming of MD lies in the time scale limitation: with today's computational resources, simulations can generally only be carried out on a time scale of nanoseconds or less. This time is too short for accurate calculations of diffusion coefficients because adequate statistics of the thermally activated atomic jumping can hardly be accumulated, especially at low temperatures. The nonequilibrium point defect concentration is another problem of MD simulations. Indeed, MD simulation runs are

often shorter than the time required for the system to generate the equilibrium concentration of point defects as defect generation is also thermally activated. With KMC simulations, the time scale limitation can be effectively overcome and diffusion coefficients can be accurately calculated. However, to use the KMC method, one must know the dominant diffusion mechanisms and construct a catalogue of all relevant atomic transitions together with their rates. The problem with this approach is that the diffusion mechanisms are often not known *a priori*. This is especially true for GB diffusion, for which the atomic mechanisms are not well established at present. In most of the previous studies the mechanism was postulated to be a simple vacancy-atom exchange, i.e., a single-atom jump into a vacant site, which can easily be studied by static calculations. Recently, Ma *et al.*<sup>8</sup> and Nomura and Adams<sup>13</sup> evaluated migration energies of interstitial and interstitialcy jumps in GB's by molecular statics, and concluded that interstitial-related mechanisms can also be important in certain cases. However, the relative importance of the vacancy and interstitial-related mechanisms has not been studied in detail, and other possible mechanisms of GB diffusion have not been explored.

The main purpose of this paper is to demonstrate an alternative approach to investigations of GB diffusion—an approach that combines the strengths of both MD and KMC methods. The procedure includes three steps. First, we use MD for the identification of GB diffusion mechanisms, including complex transitions that are difficult to guess by in-

tuition. Second, we carry out molecular statics calculations of point defect formation energies, entropies, and rate constants for the identified transitions. At this step, in contrast to previous studies,<sup>6,8,13,14</sup> we calculate the defect formation entropies and attempt frequencies directly within the harmonic approximation rather than rely on empirical correlations. Furthermore, instead of the simple “drag” method used for finding the saddle points before,<sup>6,8,13,14</sup> we apply a more reliable nudged elastic band (NEB) method<sup>15</sup> which allows us to find transition states for collective jumps involving several atoms. Third, knowing the atomic transitions and relevant point defect concentrations and rate constants, we construct KMC models based on those transitions and calculate the GB diffusion coefficients by conducting KMC simulations in a wide temperature range.

We apply this approach to studies of GB diffusion in two  $\Sigma=5$  [001] symmetric tilt GB's in Cu, one with the GB plane (210) and tilt angle  $\theta=53.1^\circ$ , and the other with the GB plane (310) and tilt angle  $\theta=36.9^\circ$ . Diffusion in these GB's has previously been studied experimentally<sup>16–18</sup> and theoretically.<sup>5–8,10</sup> Most of the previous work has been done on Ag. Our choice of Cu is motivated by its greater technological importance, particularly as a future material for advanced interconnects in microelectronic devices.<sup>19</sup> For example, electromigration damage in interconnection lines is largely determined by atomic transport along GB's, which makes GB diffusion in Cu a very attractive topic for both fundamental and applied research. As another application of our approach, we study mechanisms of spontaneous generation and annihilation of point defects in Cu GB's.

This paper is organized as follows: In Sec. II we outline our simulation methods, and in particular describe how the MD simulations were carried out, and how the point defect concentrations and migration rates were calculated. We also explain the implementation of the KMC simulations. Then in Sec. III we present the results of our GB diffusion calculations and compare them with previous theoretical and experimental studies. We also analyze point defect generation in the GB's and discuss the temperature range of applicability of our GB model. Finally, in Sec. IV, we state our conclusions.

## II. SIMULATION METHODS

### A. Interatomic potential and system geometry

The atomistic calculations reported in this paper were carried out with an embedded atom method (EAM) potential.<sup>20–22</sup> This potential was fit to accurately reproduce experimental values of the equilibrium lattice constant, cohesive energy, elastic constants, vacancy formation energy in the lattice, and other properties of Cu.

For GB simulations we used a block with a slab geometry illustrated in Fig. 1. Periodic boundary conditions were applied in the directions parallel to the GB plane. The free (dynamic) atoms were sandwiched between two slabs of fixed (static) atoms on either side of the GB plane. The dimensions of the free region were approximately equal in all three directions. The fixed atoms occupied ideal lattice positions, but the slabs themselves were allowed to move rigidly in the direction perpendicular to the GB plane during structure relaxation. The thickness of each static slab was at least

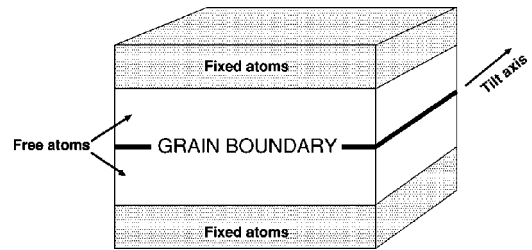


FIG. 1. Schematic geometry and boundary conditions in grain-boundary simulations.

twice the cutoff radius of atomic interaction. A GB was initially created by aligning crystallographic planes (210) or (310) parallel to the desired GB plane, followed by a  $180^\circ$  rotation of one grain relative to the other about the direction normal to the GB plane. This rotation produced a symmetric tilt coincident-site-lattice GB with the reciprocal density of coincident sites  $\Sigma=5$ .<sup>23</sup> The upper grain was then rigidly translated relative to the lower grain by different vectors parallel to the GB plane, and after each translation the system was relaxed with respect to local displacements of free atoms and rigid translations of the slabs normal to the GB. Such normal translations served to simulate a zero-pressure condition normal to the GB. By this procedure, the relaxed GB energy was examined as a function of rigid translations of the grains. For both the (210) and (310) GB's, the GB energy was found to have a single minimum. The minimum-energy configuration was identified as the ground-state structure of the GB and was used in further diffusion simulations. The relaxed structures of the GB's are shown in Fig. 2. Both GB's are made of topologically identical structural units, each representing a capped trigonal prism in three-dimensional space.<sup>23</sup> The GB's only differ in dimensions of the structural units and the way they are put together to form a periodic structure. The excess GB energies are  $937 \text{ mJ/m}^2$

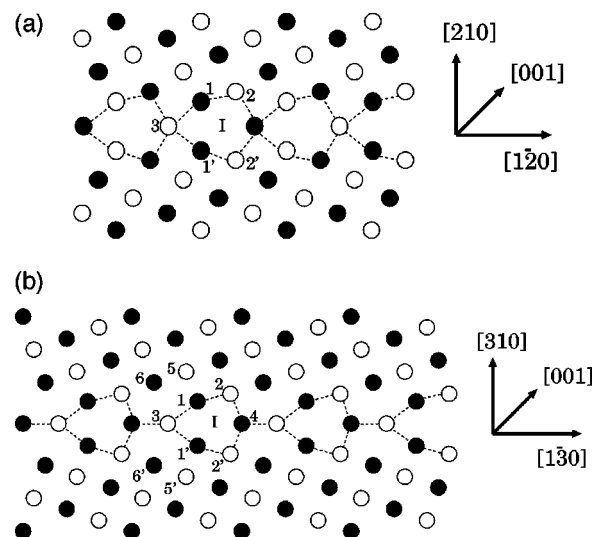


FIG. 2. Relaxed atomic structure of  $\Sigma=5$  [001] symmetric tilt GB's in Cu. (a)  $\theta=53.1^\circ$  (210) GB; (b)  $\theta=36.9^\circ$  (310) GB. Black and white circles mark atomic positions in alternating (002) planes perpendicular to the tilt axis [001]. Selected atomic sites are labeled with numbers. Symbol *I* marks an interstitial site. Dashed lines delineate structural units.

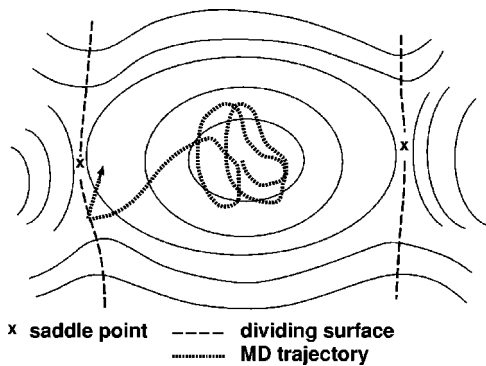


FIG. 3. Schematic illustration of the basin-constrained MD simulation technique. Whenever the system tries to escape to another state, it is reflected back into the original potential-energy basin.

for the (210) GB and 888 mJ/m<sup>2</sup> for the (310) GB. Two variants of each GB were generated: a smaller system with around 360 free atoms, and a larger system with around 1000 free atoms. The smaller system was used in MD simulations, while the larger system was used for accurate static calculations of point defect properties.

### B. Searching for diffusion mechanisms

An important step in constructing a model of GB diffusion is finding the atomic transitions by which point defects migrate in the GB. Each transition is characterized by an initial state, final state, and an intermediate transition state. The initial and final states are local minima of the potential energy in the configuration space of the system, while the transition state is a first-order saddle point. Importantly, while searching for mechanisms it is not sufficient to assume only single-atom jumps. More complex mechanisms where several atoms move in a concerted manner may also be important.

Our search for diffusion mechanisms is based on an automated procedure that was inspired by the recently proposed temperature-accelerated dynamics method.<sup>24</sup> The idea is to scan for possible transitions from a given initial state by carrying out a so-called basin-constrained MD simulation combined with searches for saddle points. The principle of a basin-constrained MD simulation is illustrated in Fig. 3. The MD trajectory is confined to a potential energy basin. Whenever the system attempts to escape to another basin, the relevant saddle point is detected, and the system is reflected back into the original basin.

The implementation of the basin-constrained MD simulation is as follows. At regular time intervals, an MD simulation is interrupted and the instantaneous atomic configuration is stored. This configuration is statically relaxed towards the minimum of the current potential energy basin. If the relaxation leads to the initial state, the system is assumed to be still in the original basin, and the MD simulation continues undisturbed from the previously stored configuration. If the relaxation leads to a new minimum, the system is assumed to have undergone a transition to a new state. In that case, we search for the saddle point between the initial and final states using the nudged elastic band (NEB) method.<sup>15</sup> Configurations from the MD trajectory are used to construct the initial

chain of configurations, which is then optimized to the minimum-energy path. The minimum-energy path is defined as a continuous path in  $3N$ -dimensional configuration space ( $N$  being the number of free atoms) with the property that at any point along the path the atomic forces are zero in the  $(3N-1)$ -dimensional hyperplane perpendicular to the path. Once the saddle point has been located, the final-state and saddle-point configurations are stored and the MD trajectory is reflected back into the original basin. This is accomplished by continuing the MD simulation from a configuration just before the transition occurred, but with the velocities of all atoms reversed. The MD simulation employs a Langevin thermostat that ensures canonical sampling and injects noise into the trajectory such that the system does not simply retrace its path backwards when the velocities are reversed.

The idea of using high-temperature MD to identify initial and final states for transitions and determining transition states using the NEB method has previously been applied to studies of the formation of mechanical contact between a metal tip and surface.<sup>25</sup> Our basin-constrained implementation of MD combined with on-the-fly transition state searches provides a convenient and automated realization of this idea. Other workers have searched for transition states in solids using mode following methods based on either diagonalization of the dynamical matrix<sup>26</sup> or iterative procedures that use only first derivatives.<sup>27,28</sup>

We assumed that GB diffusion is mediated by point defects: vacancies or interstitials. To find the diffusion mechanisms, the chosen point defect was placed at all possible positions in the GB core, and the most frequent transitions (defect jumps) from each position were identified by basin-constrained MD simulations conducted at temperature  $T = 1000$  K for 1–30 ns. To save computational time, such scans for transitions were carried out on a small system ( $\sim 360$  free atoms) with static slabs fixed in their optimum positions corresponding to the initial point defect configuration at  $T=0$ . In order to rank the observed transitions according to their importance, the migration energies and attempt frequencies were preliminary evaluated as described below (Sec. II C). Once the dominant transitions had been identified, the relevant point defect properties and rate constants were recalculated more accurately using a larger system ( $\sim 1000$  free atoms) and including rigid-body translations of the static slabs during the atomic relaxations. All point defect characteristics reported in this paper and used in the KMC simulations were obtained from the larger systems.

### C. Point defect calculations

The concentration  $c_\alpha$  of a point defect at a site  $\alpha$  in the GB core, i.e., the probability for site  $\alpha$  to be occupied by a defect, is given by

$$c_\alpha = \exp\left(-\frac{E_f^\alpha - TS_f^\alpha}{k_B T}\right), \quad (1)$$

where  $E_f^\alpha$  is the defect formation energy at site  $\alpha$ ,  $S_f^\alpha$  is the formation entropy, and  $k_B$  is the Boltzmann constant. This equation assumes that individual defects do not interact with each other.

The vacancy formation energy in a GB is defined as the energy cost of removing an atom from a certain GB site  $\alpha$

and placing it at a perfect lattice site far away from the GB. Similarly, the interstitial formation energy is defined as the energy cost of removing an atom from a perfect lattice site far away from the GB and placing it at a given interstitial site  $\alpha$  in the GB core. According to these definitions, the defect formation energy can be found as

$$E_f^\alpha = E_{GB}^\alpha - E_{GB} \pm E_{\text{bulk}}/N, \quad (2)$$

where the positive sign refers to a vacancy and the negative sign to an interstitial. In Eq. (2),  $E_{GB}^\alpha$  is the energy of a  $(N \pm 1)$ -atom simulation block with the defect at site  $\alpha$ ,  $E_{GB}$  is the energy of the initial  $N$ -atom block with a defect-free GB, and  $E_{\text{bulk}}$  is the energy of an  $N$ -atom perfect-lattice block. The energies  $E_{GB}^\alpha$  and  $E_{GB}$  must be determined after a relaxation of the block, including rigid-body translations normal to the GB plane.

A similar relation holds for defect formation entropies. In this work, defect entropies were identified with their vibrational entropies and were calculated in the classical harmonic approximation. We thus neglected the effects of lattice anharmonicity that could be significant at high temperatures, and quantum effects which could play a role at low temperatures. Possible errors arising from these approximations are probably smaller than errors arising from the interatomic potential. In the harmonic approximation, the vibrational entropy is given by the expression

$$S = k_B \sum_{i=1}^{3N} \ln \left( \frac{k_B T}{h \nu_i} \right) + 3Nk_B, \quad (3)$$

where  $\nu_i$  are the frequencies of normal atomic vibrations and  $h$  is the Planck constant. The defect formation entropies are relative entropies, i.e., they are defined through differences between entropies given by Eq. (3). When such differences are calculated, the apparent temperature dependence in Eq. (3) disappears, as does also  $h$ , as it should be in a classical theory. A calculation of normal vibrations involves a computation of the  $3N \times 3N$  dynamical matrix followed by its diagonalization. Since this is a computationally expensive procedure, we had to limit our calculations to systems with approximately 1000 atoms. To compute the vibrational entropy per atom in the perfect lattice, we used a 864-atom supercell with periodic boundary conditions in all three directions. To take into account the translational invariance of the energy of a periodic block, the three translational modes were excluded from the entropy calculations.

The rates of defect jumps were calculated using the harmonic approximation to transition state theory (TST).<sup>29</sup> In this approximation, the transition rate  $\Gamma$  is given by

$$\Gamma = \nu_0 \exp \left( - \frac{E_m}{k_B T} \right), \quad (4)$$

where  $E_m$  is the migration energy (barrier) defined as the difference in energy between the transition state and initial state, and  $\nu_0$  is an attempt frequency given by

$$\nu_0 = \frac{\prod_{i=1}^{3N} \nu_i}{\prod_{i=1}^{3N-1} \nu_i^*}. \quad (5)$$

In the numerator, the sum runs over all normal vibrational modes  $\nu_i$  of the initial state, while in the denominator it runs over all stable modes  $\nu_i^*$  of the saddle-point configuration (the unstable mode corresponding to the reaction coordinate is excluded). For each saddle-point configuration (determined as described in Sec. II B), it was verified that the atomic forces were zero and the dynamical matrix had a single negative eigenvalue, i.e., the configuration indeed represented a first-order saddle point.

#### D. KMC simulations

While the KMC method has been extensively applied for studying bulk diffusion in solids, especially in partly ordered structures (see Ref. 30 for a review), applications to GB diffusion have been initiated only recently and are still relatively scarce.<sup>8–12</sup> The KMC method allows one to calculate the diffusion coefficient of any given species once the atomic transitions, the defect concentrations, and the rate constants for defect jumps are known. Because in a residence-time implementation of the method every jump attempt is successful, statistics can be accumulated and the diffusion coefficient can be determined much more accurately than by MD simulations. In contrast to analytical calculations based on simplified models, KMC simulations include *all* jump correlation effects without any approximations. In the following we describe the implementation of the KMC method for GB diffusion in a monoatomic crystal. The approach presented here is slightly more general than previous schemes, in that it considers an arbitrary diffusion mechanism and includes collective jumps of atoms.

The GB under study is assumed to have a periodic structure consisting of identical  $n$ -atom structural units. Let each structural unit have  $n_d$  positions that support point defects participating in the chosen mechanism. These can be either interstitial positions for an interstitial-related mechanism, or some of the regular atomic positions for the vacancy mechanism. We note that even for the vacancy mechanism,  $n_d$  does not necessarily have to coincide with  $n$ . In some cases (see example in Sec. III B),  $n_d$  can be smaller than  $n$  because some atomic sites may not be able to support vacancies. The defect sites will be numbered by index  $\alpha = 1, 2, \dots, n_d$ . The probability  $c_\alpha$  that a site  $\alpha$  is occupied by a defect is given by Eq. (1). If a defect is traveling through the GB, the probability of finding it on a type- $\alpha$  site equals

$$p_\alpha = \frac{c_\alpha}{\sum_{\beta=1}^{n_d} c_\beta}. \quad (6)$$

Once at site  $\alpha$ , the defect can make one of  $k_\alpha$  different jumps, each having a rate constant (jump frequency)  $\Gamma_{\alpha j}$ ,  $j = 1, 2, \dots, k_\alpha$ , as given by Eq. (4). Let  $\vec{R}_{\alpha j}$  be the displacement vector of the defect resulting from jump  $\alpha j$ . We assume that the defect jump induces displacements of one or

more atoms. Let the elementary atomic displacement induced by a defect jump  $\alpha j$  be  $\vec{r}_{\alpha ji}$ ,  $i=1,2,\dots,l_{\alpha j}$ . Obviously,

$$\vec{R}_{\alpha j} = \pm \sum_{i=1}^{l_{\alpha j}} \vec{r}_{\alpha ji}, \quad (7)$$

where a minus sign refers to a vacancy mechanism while a plus sign corresponds to an interstitial-related mechanism. The quantities  $\{c_{\alpha}\}$ ,  $\{\Gamma_{\alpha j}\}$ , and  $\{\vec{r}_{\alpha ji}\}$ , together with period vectors of a structural unit, form a complete input data set for KMC calculations of the diffusion coefficient. This input data set is often referred to as a ‘‘KMC model’’ of diffusion.

Once a KMC model has been set, the simulations are implemented as follows. For each defect site  $\alpha$ , the residence time

$$\tau_{\alpha} = \frac{1}{k_{\alpha} \sum_{j=1} \Gamma_{\alpha j}} \quad (8)$$

and the set of local jump probabilities  $\{P_{\alpha j}\}$ , where

$$P_{\alpha j} = \tau_{\alpha} \Gamma_{\alpha j}, \quad (9)$$

are precalculated. A large simulation block consisting of  $N_s$  structural units is then created in the computer. A single point defect is created at an arbitrary site, the clock is set to zero, and the defect is released to walk through the system. At each step, the jump direction is decided by a random number according to the local jump probabilities  $\{P_{\alpha j}\}$ . The jump is implemented by updating coordinates of the defect along with the atoms that are displaced by the jump. The clock is advanced by  $\tau_{\alpha}$  and the simulation continues. Periodic boundary conditions are maintained in both directions in the GB plane, so that if a defect jumps out of the block, it reappears on its opposite border. The simulation run is divided into  $m$  individual walks, each consisting of the same number of defect jumps, so that the final configuration of the previous walk serves as the initial configuration of the new walk.

Once the simulation is complete, the diffusion coefficients of the defect and the atoms in a given direction  $x$  are calculated from the random-walk (Einstein’s) definition of a diffusion coefficient. Thus the defect diffusion coefficient is determined as

$$D_d = \frac{\sum_{k=1}^m X_k^2}{2t}, \quad (10)$$

where  $t$  is the total simulation time,  $X_k$  is the projection of the total defect displacement vector resulting from the  $k$ th walk. The atomic diffusion coefficient  $D$  is obtained by averaging over displacements of all atoms in the block:

$$D = \frac{\sum_{k=1}^m \sum_{\gamma=1}^N x_{\gamma k}^2}{2Nt} \times C_d, \quad (11)$$

$N$  being the number of atoms in the block,  $x_{\gamma k}$  the projection of the total displacement vector of the  $\gamma$ th atom resulting from the  $k$ th walk, and  $C_d$  is the average number of defects that would be in the simulation block under equilibrium conditions. (Indeed, under the simulation conditions there is always exactly one defect in the block, which generally does not correspond to the equilibrium point defect concentration at the given temperature.) The equilibrium number of defects in the block can be found from the defect occupation probabilities at different sites:

$$C_d = N_s \sum_{\alpha=1}^{n_d} c_{\alpha}. \quad (12)$$

Combining Eqs. (11) and (12) and considering that  $N \approx nN_s$  for large  $N_s$  values,<sup>31</sup> we finally have

$$D = \frac{\sum_{k=1}^m \sum_{\gamma=1}^N x_{\gamma k}^2}{2nt} \times \sum_{\alpha=1}^{n_d} c_{\alpha}. \quad (13)$$

Besides diffusion coefficients, jump correlation factors can be determined from KMC simulations. A correlation factor is defined as the ratio of the actual diffusion coefficient to a so-called uncorrelated diffusion coefficient calculated under the assumption that all jumps are statistically independent of one another. Thus, for the correlation factors of the defect  $f_d$  and atoms  $f$ , we have

$$f_d = \frac{D_d}{D_d^*}, \quad f = \frac{D}{D^*}, \quad (14)$$

where  $D_d^*$  and  $D^*$  are the uncorrelated diffusion coefficients. While defect jumps in a perfect lattice are totally independent of each other, so that  $f_d = 1$ , defect jumps in GB’s can be correlated.<sup>10,11</sup> The strength of such ‘‘structural’’ correlations depends on the particular GB structure and diffusion direction. For example, if there is a pair of sites with a low-energy barrier for defect jumps between them, a defect may get trapped and jump many times back and forth between such sites without any advancement in the diffusion direction. If the jumps between the two sites have a nonzero projection in the diffusion direction, the multiple jump reverses will obviously result in  $f_d < 1$ . For atomic diffusion, even lattice diffusion by the vacancy mechanism is correlated with  $f < 1$ .<sup>32</sup> Indeed, if an atom exchanges with a ‘‘fresh’’ vacancy approaching the atom from a random direction, all possible atomic jumps have an equal probability of  $1/z$ ,  $z$  being the number of first neighbors. However, after this first jump the vacancy remains in a neighbor position of the atom and modifies the symmetry of the next-jump probabilities of the atoms. Namely, there is a finite probability that the next atomic jump will be induced by the same vacancy after it makes some number of jumps near the atom. Because the vacancy is initially behind the atom, the atomic jumps whose projections on the previous jump direction are negative will obviously occur with larger-than-random probabilities ( $> 1/z$ ) while jumps whose projections are positive will occur with smaller-than-random probabilities ( $< 1/z$ ). In GB

diffusion, such ‘‘defect-induced’’ correlations can be stronger, and in addition may depend on temperature.<sup>10,11</sup>

Uncorrelated diffusion coefficients can be calculated in two ways. First, the sums appearing in Eqs. (10) and (13) can be replaced by sums of squared projections of all elementary defect (respectively, atomic) jumps that happened during the simulation time. Such sums can be easily accumulated in the course of the KMC simulation. Second,  $D_d^*$  and  $D^*$  can be calculated *a priori* as

$$D_d^* = \frac{1}{2} \sum_{\alpha=1}^{n_d} \sum_{j=1}^{k_\alpha} p_\alpha \Gamma_{\alpha j} \Lambda_{\alpha j}^2, \quad (15)$$

and

$$D^* = \frac{1}{2n} \sum_{\alpha=1}^{n_d} \sum_{j=1}^{k_\alpha} \sum_{i=1}^{l_{\alpha j}} c_\alpha \Gamma_{\alpha j} \lambda_{\alpha ji}^2, \quad (16)$$

respectively. In these equations,  $\Lambda_{\alpha j}$  and  $\lambda_{\alpha ji}$  are  $x$  projections of the elementary jump vectors  $\vec{R}_{\alpha j}$  and  $\vec{r}_{\alpha ji}$ , respectively. Because all jumps are assumed to be independent of one another, the squared projections enter Eqs. (15) and (16) with weights proportional the corresponding jump rates  $c_\alpha \Gamma_{\alpha j}$ .

In this work, the uncorrelated diffusion coefficients were calculated both ways, and the agreement between the calculations served as one of the tests that all jumps included in the KMC model were properly sampled by the simulation. As a more detailed test, the occurrences of different types of jumps were counted in the course of the simulations, and the obtained average jump rates were compared with their *a priori* estimates  $c_\alpha \Gamma_{\alpha j}$ . In addition, in each run the average atomic displacement was computed and checked to be much smaller than the root-mean-squared displacement, as it should be for a random walk without external forces. At several temperatures, diffusion calculations were performed with different simulation times and block sizes in order to check the convergence. The total number of defect jumps in a run was typically around  $10^{12}$  for high temperatures but significantly larger (up to  $10^{14}$ ) for low temperatures.

### III. RESULTS AND DISCUSSION

#### A. Diffusion in Cu lattice

To put our GB diffusion results into perspective, we started out by investigating diffusion of vacancies and self-interstitials in the Cu lattice using the same techniques as we applied for GB diffusion. It was found, as expected, that a vacancy moves by simple vacancy-atom exchanges. For a self-interstitial, a split [001] dumbbell configuration was found to be the lowest energy configuration. This dumbbell was established to move by translating the center of mass by one nearest-neighbor distance and simultaneously rotating by  $90^\circ$ . This interstitial migration mechanism is identical to the one reported recently by Zhao and Shimomura<sup>33</sup> based on calculations with the EAM potential of Daw and Baskes.<sup>34</sup> The same mechanism was earlier found by Johnson and Brown<sup>35</sup> using pair potentials and by Wales and Uppenbrink<sup>26</sup> using a Sutton-Chen potential for Ag. We note that this mechanism is at variance with the one reported recently by Tajima *et al.*<sup>36</sup> who employed a less tested EAM

TABLE I. Calculated characteristics of point defect formation and migration in Cu lattice. Experimental data are given in parentheses.

Defect	$E_f$ (eV)	$S_f/k_B$	$E_m$ (eV)	$\nu_0$ (THz)
Vacancy	1.258 (1.27 <sup>a</sup> ; 1.28 <sup>b</sup> )	1.23 (2.35 <sup>b</sup> )	0.690 (0.71 <sup>b</sup> )	5.3
Interstitial	3.229	11.01	0.083 (0.12 <sup>c</sup> )	1.0

<sup>a</sup>Reference 37.

<sup>b</sup>Reference 38.

<sup>c</sup>Reference 39.

potential and found that interstitial migration occurred through a body-centered configuration as a saddle point. Our simulations did not confirm that mechanism.

The vacancy and interstitial properties were calculated on a periodic lattice block with  $\sim 864$  atoms. The volume of the block was allowed to vary during the energy minimization in order to simulate zero pressure conditions. The results, which are summarized in Table I, compare reasonably well with experimental data known to us.<sup>37-39</sup> Even though the interstitial migration energy is relatively low, the formation energy is very high and lattice diffusion is obviously dominated by vacancies. The lattice diffusion coefficient by the vacancy mechanism can be calculated as<sup>40</sup>

$$D = D_0 \exp\left(-\frac{Q}{k_B T}\right) \quad (17)$$

with the activation energy  $Q = E_f + E_m$  and the pre-exponential factor  $D_0 = f_0 a^2 \nu_0 \exp(S_f/k_B)$ . Here,  $a = 3.615$  Å is the lattice constant and  $f_0 \approx 0.7815$  is the correlation factor for self-diffusion in a face-centered-cubic lattice. Using the data from Table I we find  $D_0 = 0.2 \times 10^{-5}$  m<sup>2</sup>/s and  $Q = 1.95$  eV. These numbers are in reasonable agreement with experimental data measured by the radiotracer method in several studies,<sup>41</sup> for example  $D_0 \sim 10^{-5}$  m<sup>2</sup>/s and  $Q = 2.03$  eV.<sup>42</sup>

#### B. Point defect formation in grain boundaries

Point defect formation energies and entropies at selected sites in the two GB's were calculated using the procedures

TABLE II. Energy ( $E_f$ ) and entropy ( $S_f$ ) of defect formation at different GB sites. See Fig. 2 for site numbering.

GB	Defect	Site	$E_f$ (eV)	$S_f/k_B$
(210)	vacancy	1	0.316	2.59
		2	0.544	5.13
		3	1.338	0.75
(310)	vacancy	<i>I</i>	0.245	-2.14
		1	0.644	0.30
		2	1.075	2.92
		3	1.353	0.71
		4	0.777	1.37
	interstitial	5	0.997	1.07
		<i>I</i>	0.231	-0.06

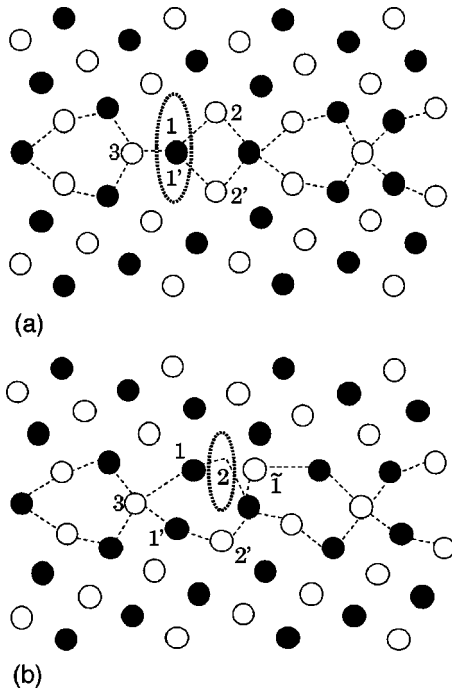


FIG. 4. Relaxed structure of the  $\Sigma=5$  (210)[001] GB with a vacancy. Only projections of the (002) plane containing the vacancy and an adjacent (002) plane are shown. The dotted oval marks the vacant site. (a) Vacancy at site 1. The atom initially at site 1' relaxes to the GB plane. (b) Vacancy at site 2. The atoms initially at site 1 of the same structural unit and site  $\bar{1}$  of the neighboring structural unit strongly relax towards the vacancy.

described in Sec. II C and the results are listed in Table II. In each of the GB's, there is one uniquely preferred type of interstitial site (called  $I$ ) located in the center of the triangle formed by atoms 2, 2', and 3 (see Fig. 2). This site is in the largest open region in the GB core. Vacancy formation energies vary widely from site to site, as do also the formation entropies. The table illustrates that defect formation energies in the GB core can be much lower than in the bulk, especially for interstitials, which is one of the main reasons for the enhanced GB diffusion. It should be noted, however, that some GB sites, like site 3, have a higher vacancy formation energy than a perfect lattice site. An interesting observation is that site 6 in the (310) GB does not support vacancies at all: when an atom is removed from that site to form a vacancy, the atom located in the nearest site 1 fills the vacancy during the relaxation process, so that the vacancy effectively moves (relaxes) to site 1. We believe that this finding represents a general phenomenon, namely, that certain sites in GB's (and perhaps in extended defects in general) are not able to support vacancies. Even more interestingly, the existence of such *unstable vacancies* has a strong impact on atomic mechanisms of diffusion, as will be shown below.

Atoms surrounding a vacancy in a GB may relax quite significantly, as illustrated in Fig. 4 for the (210) GB. For example, when a vacancy is created at site 1, the atom previously located at the symmetrical site 1' relaxes towards the GB plane and finds its equilibrium position exactly in the middle between the initial sites 1 and 1' [Fig. 4(a)]. The same relaxed structure can be obtained by creating a vacancy at site 1'. This example illustrates the effect of *vacancy de-*

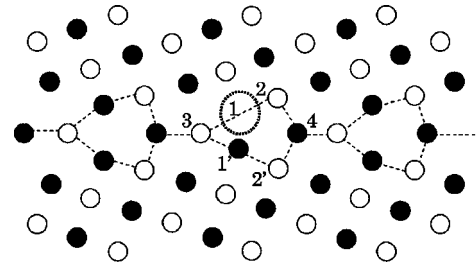


FIG. 5. Relaxed structure of the  $\Sigma=5$  (310)[001] GB with a vacancy at site 1. Only projections of the (002) plane containing the vacancy and an adjacent (002) plane are shown. The dotted oval marks the vacant site. Relaxations around the vacant site are relatively small.

*localization* in GB's, which we believe is another important general phenomenon in high-angle GB's. In this particular case, the free volume associated with the vacancy is, in effect, shared by sites 1 and 1', so that the vacancy cannot be identified as located at either one of these sites. The vacancy at site 2 is also associated with large relaxations [Fig. 4(b)]. In this case, atom 1 of the same structural unit and atom  $\bar{1}$  of the neighboring structural unit relax significantly towards the vacant site, but the vacancy can still be considered as localized at site 2. Note that the relaxation pattern in the neighboring structural unit is very similar to that induced by a vacancy at site  $\bar{1}$  [cf. Fig. 4(a)]. In other words, the atomic relaxations “prepare” the GB structure for a vacancy jump from site 2 to sites 1 or  $\bar{1}$ . From this observation we could already expect that the barriers for those jumps must be very low, which is indeed confirmed by calculations (see below). In the (310) GB, all vacancies are well localized at atomic sites and relaxations are relatively small. As an example, the relaxed GB structure with a vacancy at site 1 is shown in Fig. 5.

### C. Dominant diffusion mechanisms

As a result of the MD simulations described in Sec. II B, we chose a set of the most probable transitions involving vacancies and self-interstitials in both GB's. Assuming that those transitions dominate atomic diffusion in the GB's, we have investigated them in detail and used them in KMC simulations. In what follows we will describe those transitions and report their migration energies, attempt frequencies, and other characteristics.

#### 1. Vacancy migration

Vacancy transitions included in the KMC simulations are illustrated in Fig. 6 and the migration parameters are listed in Table III. The table includes the reverse transitions unless the initial and final states are symmetrically equivalent. Such reverse transitions are not shown in Fig. 6, but they were of course included in the KMC simulations. The last column in Table III gives so-called “partial” activation energies,  $E_f + E_m$ , which are useful for ranking the relative importance of individual transitions, since  $c_\alpha \Gamma_{\alpha j} \propto \exp[-(E_f + E_m^\alpha)/k_B T]$ . Transitions with lower partial activation energies are expected to occur more often.

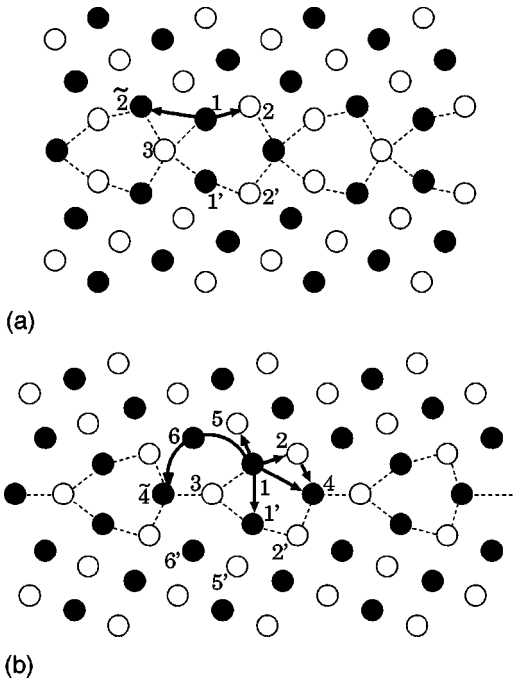


FIG. 6. Vacancy transitions in  $\Sigma=5$  [001] GB's. Only transitions included in the KMC model are shown. (a)  $\theta=53.1^\circ$  (210) GB. (b)  $\theta=36.9^\circ$  (310) GB. A tilde sign over a number marks an equivalent site in a neighboring structural unit. Transitions are only shown in one direction, but the reverse transitions are of course also included in the KMC model. Note that the pictures are schematic in that the arrows connect nonrelaxed vacancy sites. For instance, transition  $1 \rightarrow 2$  in (a) indicates a jump of a vacancy from site 1 [structure shown in Fig. 4(a)] to site 2 [structure shown in Fig. 4(b)]. Migration energies and attempt frequencies are listed in Table III.

For the (210) GB [Fig. 6(a)], we include two vacancy jumps between sites 1 and 2. Both jumps are simple vacancy-atom exchanges. The first jump,  $1 \rightarrow 2$ , has a component  $\frac{1}{2}[001]$  along the tilt axis and can contribute to diffusion in both directions in the GB plane. The second jump,  $1 \rightarrow \tilde{2}$ , bridges two neighboring structural units. The jump vector is normal to the tilt axis, so this jump does not contribute to diffusion along the tilt axis. The barriers of the reverse jumps,  $2 \rightarrow 1$  and  $\tilde{2} \rightarrow 1$ , are very low (Table III), which correlates with the relaxation pattern around the vacancy at site 2 as discussed above [see Fig. 4(b)]. Although the vacancy at site 2 is formally stable, it is short-lived and almost acts as a transition state for transitions between type-1 sites of neighboring structural units.

For the (310) GB, we include several vacancy transitions shown in Fig. 6(b). All but one of them are simple vacancy-atom exchanges. The exception is the transition  $1 \rightarrow 6 \rightarrow \tilde{4}$  that involves a concerted motion of two atoms. In this transition, atom 6 moves towards the vacant site 1 while atom  $\tilde{4}$  simultaneously moves towards site 6, until finally atom 6 fills the vacancy while atom  $\tilde{4}$  takes its place and leaves a vacancy behind. Importantly, this “long” vacancy jump could not be implemented as a sequence of two elementary jumps,  $1 \rightarrow 6$  and  $6 \rightarrow \tilde{4}$ , as the vacancy at site 6 is unstable. In this sense, it is the vacancy instability that causes “long” vacancy jumps involving concerted motion of two atoms. It should be pointed out that this transition is an important part of the KMC model since it is the easiest transition that bridges neighboring structural units and thereby provides long-range vacancy diffusion perpendicular to the tilt axis.

Previously, Ma *et al.* studied vacancy transitions in the same (310) GB in Ag.<sup>8</sup> They identified the easiest transitions

TABLE III. Migration energies  $E_m$ , attempt frequencies  $\nu_0$ , and partial activation energies  $E_f + E_m$  of transitions included in the KMC models. For transitions in which the initial and final states are nonequivalent, the reverse transitions are also included. Defect jumps can be parallel ( $\parallel$ ) or perpendicular ( $\perp$ ) to the tilt axis, or may have both components ( $\parallel + \perp$ ). Transitions are shown in Figs. 6 and 7.

GB	Defect	Transition	Direction	$E_m$ (eV)	$\nu_0$ (THz)	$E_f + E_m$ (eV)
(210)	vacancy	$1 \rightarrow 2$	$\parallel + \perp$	0.255	6.56	0.571
		reverse	$\parallel + \perp$	0.027	0.52	0.571
		$1 \rightarrow \tilde{2}$	$\perp$	0.231	7.38	0.546
		reverse	$\perp$	0.002	0.59	0.546
	interstitial	$I \rightarrow 1 \rightarrow I^*$	$\parallel$	0.481	12.82	0.726
		$I \rightarrow \tilde{3} \rightarrow \tilde{I}$	$\parallel + \perp$	0.629	27.36	0.874
(310)	vacancy	$1 \rightarrow 1'$		0.042	4.65	0.686
		$1 \rightarrow 2$	$\parallel + \perp$	0.477	41.82	1.121
		reverse	$\parallel + \perp$	0.046	3.02	1.121
		$1 \rightarrow 4$	$\perp$	0.609	6.84	1.253
		reverse	$\perp$	0.477	2.34	1.253
		$1 \rightarrow 6 \rightarrow \tilde{4}$	$\perp$	0.488	10.9	1.133
		reverse	$\perp$	0.356	3.73	1.133
		$1 \rightarrow 5$	$\parallel + \perp$	0.416	0.99	1.060
		reverse	$\parallel + \perp$	0.063	0.46	1.060
		$2 \rightarrow 4$	$\parallel + \perp$	0.053	1.32	1.128
	reverse	$\parallel + \perp$	0.351	6.27	1.128	
	interstitial	$I \rightarrow 1 \rightarrow I^*$	$\parallel$	0.290	2.09	0.521
		$I \rightarrow 2 \rightarrow \tilde{3} \rightarrow \tilde{I}$	$\perp$	0.576	1.38	0.735

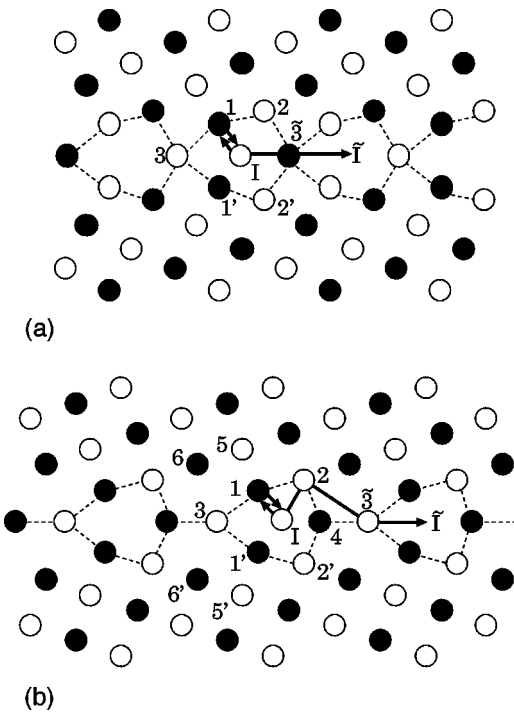


FIG. 7. Interstitial transitions in  $\Sigma = 5$  [001] GB's. Only transitions included in the KMC model are shown. (a)  $\theta = 53.1^\circ$  (210) GB. (b)  $\theta = 36.9^\circ$  (310) GB. A tilde sign over a number marks an equivalent site in a neighboring structural unit. Migration energies and attempt frequencies are listed in Table III.

by trying various single-atom jumps using molecular statics and the “drag” method. Some of the jumps found by Ma *et al.* coincide with ours, but there are some differences. While Ma *et al.* evaluated vacancy jumps involving site 3 as important for diffusion, we find that such jumps are of negligible importance because of the high vacancy formation energy at site 3. On the other hand, sites 5 and 6 that we find to play an important role in vacancy diffusion were not considered by Ma *et al.* The “long” vacancy jump  $1 \rightarrow 6 \rightarrow \bar{4}$  that provides the main contribution to vacancy diffusion perpendicular to the tilt axis was not identified by Ma *et al.* They also found vacancy jumps [001] between symmetrically equivalent sites in adjacent (001) planes to be relatively easy. According to our calculations, such direct jumps have high barriers or decompose into pairs of easier jumps between neighboring (002) planes. For example, for a vacancy at site 1 it is easier to make two jumps,  $1 \rightarrow 5$  and  $5 \rightarrow 1^*$ , than a direct jump  $1 \rightarrow 1^*$  with a barrier of 0.680 eV (an asterisk marks equivalent sites in adjacent (001) planes). Such direct jumps were found to be unfavorable in the (210) GB too. Some of the discussed differences can be attributed to the fact that we studied a different metal with a different potential. But it is also important to recognize that effects like “long” vacancy jumps could hardly be identified with simulation methods used previously.

## 2. Interstitial migration

Diffusion mechanisms involving interstitials are traditionally divided in two categories:<sup>40</sup> (i) the direct interstitial mechanism, in which an interstitial atom jumps directly from site to site while the other atoms remain at their respective

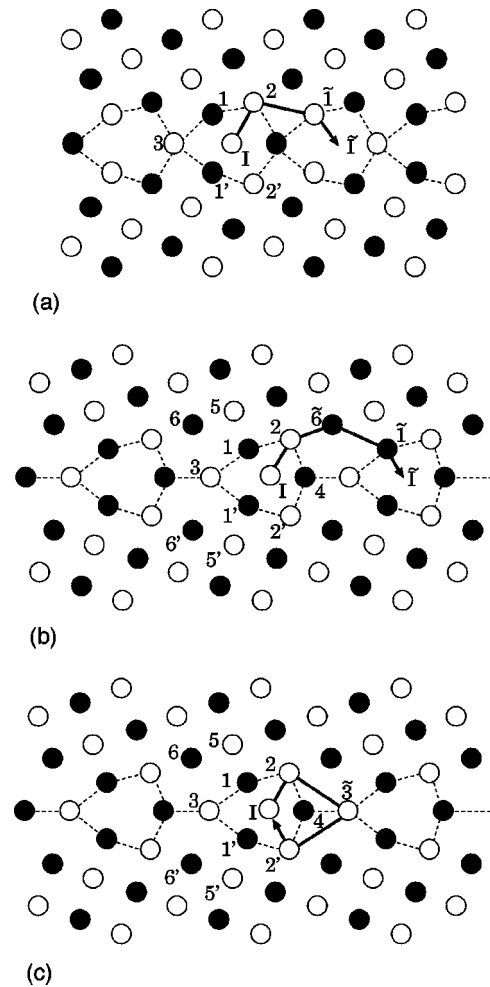


FIG. 8. More complex interstitial transitions that are not included in the KMC model. (a) Long interstitial jump in the (210)[001] GB. (b) Long interstitial jump in the (310)[001] GB. (c) Ring process in the (310)[001] GB. A tilde sign over a number marks an equivalent site in a neighboring structural unit.

sites, and (ii) the interstitialcy mechanism, in which an interstitial atom kicks a lattice atom out of its regular position to another interstitial site and takes its place. This latter mechanism obviously involves a concerted motion of two atoms. The interstitialcy mechanism is known for bulk diffusion in certain ionic compounds.<sup>40</sup>

In both  $\Sigma = 5$  [001] tilt GB's, diffusion of interstitials was found to occur predominantly by the interstitialcy mechanism. The easiest interstitialcy jumps are shown in Fig. 7 and listed in Table III. In both GB's, diffusion parallel to the tilt axis can be provided by the interstitialcy jump  $I \rightarrow 1 \rightarrow I^*$  between symmetrically equivalent interstitial sites  $I$  and  $I^*$  (jump vector [001]). In such transitions the interstitial atom located initially at site  $I$  kicks atom 1 out to site  $I^*$  and takes its place. For diffusion perpendicular to the tilt axis, the easiest transitions are  $I \rightarrow \bar{3} \rightarrow \bar{I}$  in the (210) GB [Fig. 7(a)] and  $I \rightarrow 2 \rightarrow \bar{3} \rightarrow \bar{I}$  in the (310) GB [Fig. 7(b)]. While the first transition matches the classical definition of the interstitialcy mechanism,<sup>40</sup> the second one is more complex, in that it involves a concerted motion of three atoms.

Direct interstitial jumps were also studied, but were found not to be favorable for these GB's: they had a high barrier or

TABLE IV. Energy barriers of complex interstitial-related and ring mechanisms. Transitions are shown in Figs. 8 and 9.

GB	Transition	Direction	$E_m$ (eV)	Figure
(210)	$I \rightarrow 2 \rightarrow \tilde{I} \rightarrow \tilde{I}$	$\parallel + \perp$	0.689	8(a)
	$1 \rightarrow 2 \rightarrow \tilde{I} \rightarrow \tilde{2} \rightarrow \tilde{I} \rightarrow 2 \rightarrow 1$	ring	0.987	9
(310)	$I \rightarrow 2 \rightarrow \tilde{6} \rightarrow \tilde{I} \rightarrow \tilde{I}$	$\perp$	0.818	8(b)
	$I \rightarrow 2 \rightarrow \tilde{3} \rightarrow 2' \rightarrow I$	ring	0.641	8(c)

dissociated into easier transitions shown in Fig. 7. Comparing these findings with previous work, the interstitialcy jump  $I \rightarrow 1 \rightarrow I^*$  was considered for diffusion parallel to the tilt axis in the (310) GB in Ag.<sup>8</sup>

#### D. Complex mechanisms

Besides the dominant transitions shown in Figs. 6 and 7 and used in our KMC simulations, the MD simulations revealed a number of other transitions whose migration energies are higher but still low enough that they might be important in some cases. Typically, such transitions are more complex and involve a concerted motion of 3–4 atoms. Some examples involving interstitials are shown in Fig. 8, and the migration energies are listed in Table IV. In the (210) GB, there is a three-atom interstitialcy jump  $I \rightarrow 2 \rightarrow \tilde{I} \rightarrow \tilde{I}$  [Fig. 8(a)] that induces the same displacement of the interstitial as the dominant two-atom interstitialcy jump  $I \rightarrow \tilde{3} \rightarrow \tilde{I}$  [cf. Fig. 7(a)] but has a higher migration energy of 0.689 eV. In the (310) GB, we found an interstitialcy jump  $I \rightarrow 2 \rightarrow \tilde{6} \rightarrow \tilde{I} \rightarrow \tilde{I}$  involving four atoms [Fig. 8(b)]. The net interstitial displacement is the same as in the three-atom transition  $I \rightarrow 2 \rightarrow \tilde{3} \rightarrow \tilde{I}$  [cf. Fig. 7(b)], but the migration energy (0.818 eV) is higher.

Another class of complex mechanisms is represented by ring processes. As an example, Fig. 8(c) shows a ring process involving three regular atoms and one interstitial in the (310) GB. The energy barrier is moderate, 0.641 eV, so it is

conceivable that this process can play a role at high temperatures. Although the interstitial returns to its initial position, the four atoms exchange their sites. Thus even though repeated ring processes of this type do not provide a net mass transport along the GB, they intermix atoms and thus can contribute to tracer diffusion or diffusion of impurity atoms. A more complex ring process, found in a defect-free (210) GB, is shown in Fig. 9. In this case, six atoms in three sequential (002) planes exchange sites in a ringlike manner. Again, although the energy barrier of this process, 0.987 eV, is relatively high, this process can still play a role at high temperatures. Because this transition does not require any pre-existing point defects, this energy barrier coincides with the activation energy of diffusion.

For lattice diffusion in solids, ring mechanisms were first proposed by Zener<sup>43</sup> and have been discussed in the literature for many years.<sup>40,44</sup> However, because such mechanisms have never been detected experimentally or reliably established by simulations, they have always been considered as possible geometrically but very difficult energetically. Our simulations provide evidence that ring mechanisms can operate in GB's, and we believe that they can be found in other extended defects too.

#### E. Diffusion coefficients and correlation factors

Diffusion coefficients of vacancies, interstitials, and atoms by the vacancy and interstitialcy mechanisms were calculated by KMC simulations as described in Sec. II D. The KMC input data sets were generated using the point defect properties summarized in Tables II and III. Only transitions shown in Figs. 6 and 7 were included in the KMC models. The diffusion coefficients and correlation factors were determined for diffusion both parallel and perpendicular to the tilt axis. The calculations were performed at temperatures from 300 to 1100 K.

The obtained atomic diffusion coefficients are summarized as Arrhenius diagrams in Fig. 10. It is immediately seen that the diffusion coefficients follow the Arrhenius law quite accurately in a wide temperature range. The Arrhenius parameters obtained by fitting Eq. (17) to the data in Fig. 10 are listed in Table V. The compliance of the diffusion coefficients with the Arrhenius law indicates that, despite the presence of several transitions with different partial activation energies, the overall diffusion is dominated by either one transition or several transitions with nearly identical partial activation energies. In most cases, such dominant transition can be identified by comparing the partial and apparent activation energies in Tables III and V. For example, diffusion by the interstitialcy mechanism along the tilt axis in both GB's is obviously dominated by  $I \rightarrow 1 \rightarrow I^*$  transitions. Diffusion by the vacancy mechanism in the (310) GB is controlled by transitions  $1 \rightarrow 2$ ,  $1 \rightarrow 5$ ,  $2 \rightarrow 4$ , and  $1 \rightarrow 6 \rightarrow \tilde{4}$  having similar partial activation energies of  $\sim 1.1$  eV. A less clear case is diffusion by the interstitialcy mechanism perpendicular to the tilt axis in the (310) GB, in which the apparent activation energy  $Q = 0.804$  eV is noticeably higher than the partial activation energy 0.735 eV. This discrepancy

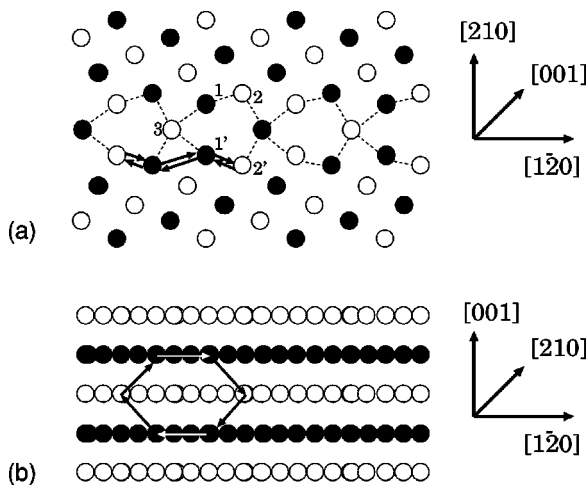


FIG. 9. Ring process in the defect-free (210)[001] GB. The arrows show displacements of atoms. Two projections of the GB structure are shown: (a) Projection normal to the GB plane. (b) Projection parallel to the GB plane.

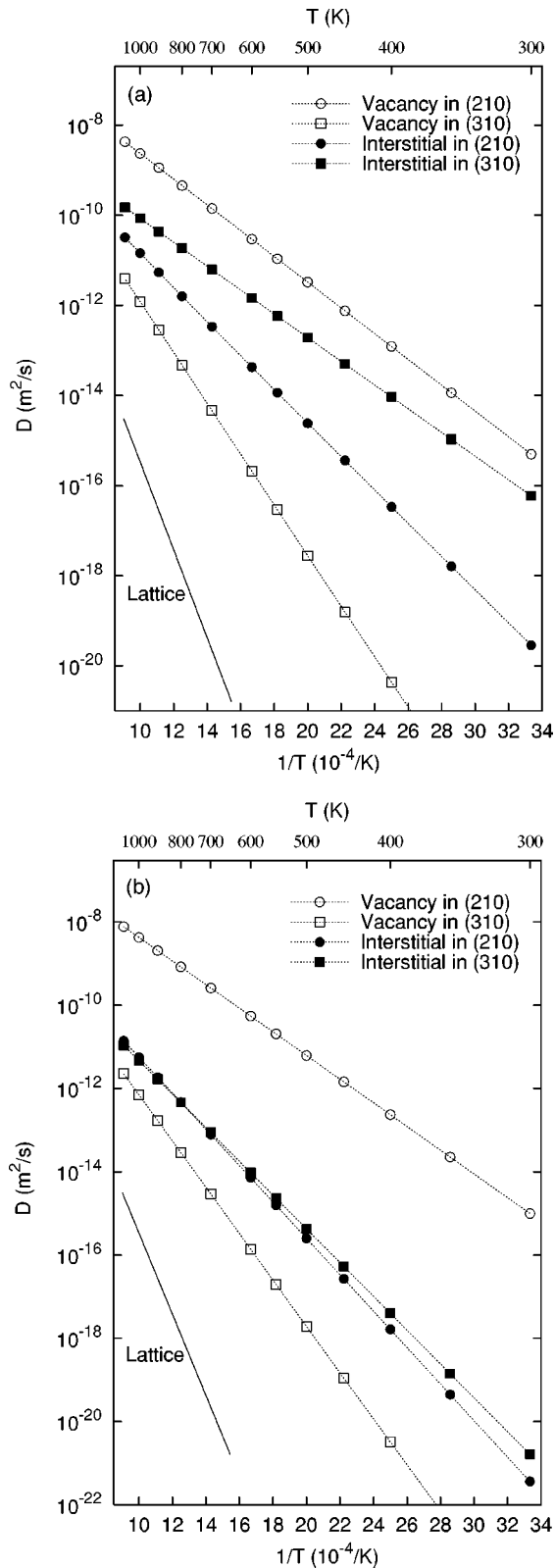


FIG. 10. Arrhenius plots of atomic GB diffusion coefficients obtained by KMC simulations. (a) Diffusion parallel to the tilt axis. (b) Diffusion perpendicular to the tilt axis. The diffusion coefficients in the perfect lattice are shown for comparison.

has to do with a trapping effect for atomic diffusion perpendicular to the tilt axis, as will be explained below.

Figure 10 also shows that, regardless of the diffusion direction, diffusion in the (210) GB is dominated by the va-

TABLE V. Arrhenius parameters of GB diffusion in Cu obtained by fitting Eq. (17) to KMC results.

GB	Mechanism	Direction	$Q$ (eV)	$D_0$ ( $\text{m}^2/\text{s}$ )
(210)	vacancy	$\parallel$	0.567	$1.71 \times 10^{-6}$
		$\perp$	0.564	$2.97 \times 10^{-6}$
	interstitialcy	$\parallel$	0.741	$0.75 \times 10^{-7}$
		$\perp$	0.867	$1.34 \times 10^{-7}$
(310)	vacancy	$\parallel$	1.112	$4.73 \times 10^{-7}$
		$\perp$	1.101	$2.50 \times 10^{-7}$
	interstitialcy	$\parallel$	0.524	$0.37 \times 10^{-7}$
		$\perp$	0.804	$0.53 \times 10^{-7}$

cancy mechanism while diffusion in the (310) GB is dominated by the interstitialcy mechanism. The anisotropy of GB diffusion is small in the (210) GB and significant, especially at low temperatures, in the (310) GB. At all temperatures studied, diffusion in the (210) GB is faster than in the (310) GB, especially in the direction normal to the tilt axis. Note that the slower diffusion rates and stronger anisotropy in the (310) GB in comparison with the (210) GB correlate with its lower energy. It is known that high-energy GB's tend to have larger diffusion coefficients and smaller anisotropy than low-energy GB's.<sup>1,2</sup>

Jump-correlation factors of point defects and atoms were calculated from Eqs. (14) and examined as functions of temperature. As expected, correlation factors of interstitials were found to be equal to unity regardless of the GB structure or diffusion direction. For vacancies in the (210) GB, the correlation factor is also close to unity in both directions, again as expected because vacancies effectively jump between type-1 sites forming a network topologically equivalent to a square lattice. For vacancies in the (310) GB, the correlation factor is again close to unity for diffusion parallel to the tilt

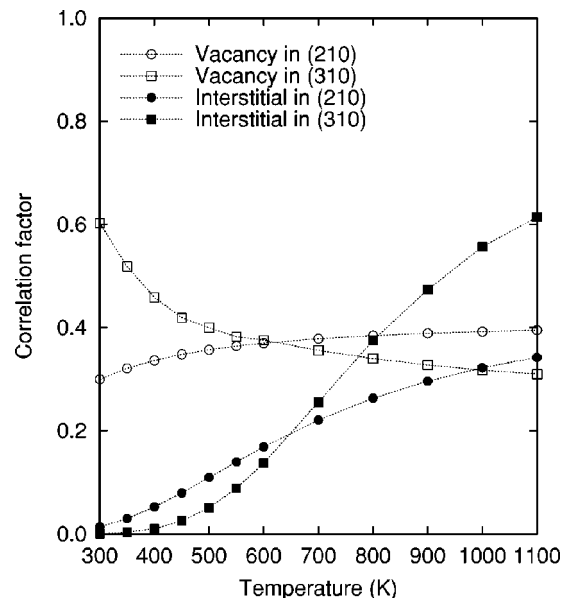


FIG. 11. Atomic correlation factors for diffusion by the vacancy and interstitialcy mechanisms perpendicular to the  $[001]$  tilt axis in the  $\Sigma=5$  (210) and (310) GB's.

axis, but varies between 0.50 at 300 K and 0.65 at 1100 K for diffusion perpendicular to the tilt axis. Regarding atomic correlation factors, for the vacancy mechanism they were found to vary between 0.3 and 0.6 depending on the GB structure, diffusion direction and temperature. This behavior is at variance with earlier KMC calculations for the (310) GB in Ag, in which the atomic correlation factor showed a more significant temperature dependence and anisotropy.<sup>10</sup> This difference is not surprising because input data sets for KMC simulations in Ag and Cu were significantly different as discussed in Sec. III C 1. For diffusion by the interstitialcy mechanism, the atomic correlation factor was observed to strongly depend on the diffusion direction. For atomic diffusion parallel to the tilt axis, the correlation factor was found to vary with temperature between 0.65 and 0.85 in both GB's. In contrast, for atomic diffusion perpendicular to the tilt axis the correlation factor is small at low temperatures but increases rapidly with temperature, especially in the (310) GB (Fig. 11).

The small correlation factors for atomic diffusion by the interstitialcy mechanism at low temperatures can be explained by a *trapping effect*. Indeed, because interstitialcy jumps  $I \rightarrow 1 \rightarrow I^*$  along the tilt axis are much easier than jumps perpendicular to the tilt axis, an interstitial makes many jumps along the tilt axis before it makes one jump in the normal directions. From the point of view of interstitial diffusion, these fast jumps parallel to the tilt axis are decoupled from the jumps perpendicular to the tilt axis and do not affect the correlation factor. However, the *atomic* jumps induced by the  $I \rightarrow 1 \rightarrow I^*$  transitions do have components normal to the tilt axis, and these normal components repeatedly cancel each other as an interstitial makes jumps along the tilt axis. This produces a trapping effect for atomic diffusion normal to the tilt axis. As the temperature increases, the interstitial jump rates become more isotropic and the trapping effect decreases. The strong retardation of low-temperature diffusion due to atomic jump correlations can cause an increase in the apparent activation energy of diffusion over the partial activation energy of the respective interstitial jump. This effect is especially pronounced in the (310) GB and explains the discrepancy between the partial activation energy and the apparent activation energy for atomic diffusion perpendicular to the tilt axis. The trapping effect becomes weaker at high temperatures.

#### F. Comparison with experiments

Experimental diffusion measurements have recently been carried out for the  $\Sigma = 5$  tilt GB's studied in this work.<sup>16-18</sup> In particular, radiotracer measurements have been made on the (210) and (310) GB's in Ag bicrystals. Although a quantitative comparison with our results, obtained for Cu, would not be justified, we would like to point out that, in agreement with our calculations, the experiments also revealed a higher diffusivity in the (210) GB than the (310) GB.

Budke *et al.*<sup>18</sup> studied Au radiotracer diffusion in a series of Cu bicrystals with orientations around the (310)[001] tilt GB at several temperatures. They found that the GB diffusivity parallel to the tilt axis attained a minimum at an orientation approximately corresponding to the ideal  $\Sigma = 5$  orientation with  $\theta = 36.9^\circ$ . Moreover, at  $T = 919$  K Budke *et al.*

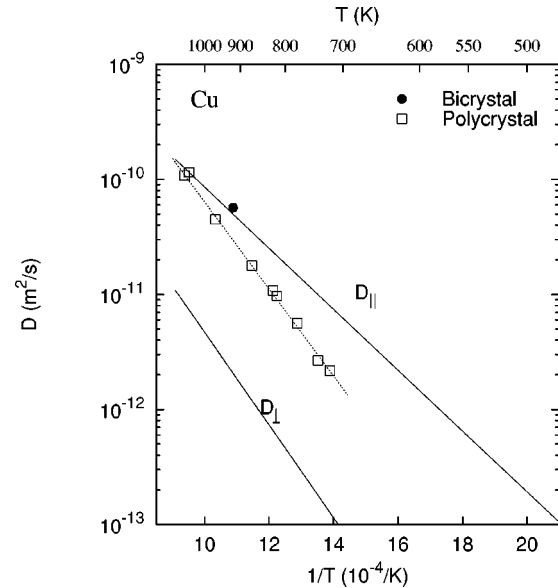


FIG. 12. Calculated atomic diffusion coefficients parallel ( $D_{\parallel}$ ) and perpendicular ( $D_{\perp}$ ) to the [001] tilt axis in the  $\Sigma = 5$  (310) GB in Cu in comparison with experimental data. Experimental data: (●) diffusion in a Cu bicrystal parallel to the tilt axis (Ref. 18), (□) diffusion in a Cu polycrystal (Ref. 45). Because experiments measure the product  $D\delta$ , the GB width  $\delta$  was assumed to be 1 nm.

performed Cu self-diffusion measurements in the same set of GB's using the radiotracer  $^{64}\text{Cu}$ . They found again a minimum of GB diffusivity at  $\theta \sim 36.3^\circ$  with  $D\delta = 5.68 \times 10^{-20}$  m<sup>3</sup>/s, where  $\delta$  is the GB width. Experiments can only give the product  $D\delta$  and not  $D$  and  $\delta$  separately. Using the traditional assumption of  $\delta = 1$  nm,<sup>1</sup> we estimate  $D = 5.68 \times 10^{-11}$  m<sup>2</sup>/s, which compares quite well with our calculations (Fig. 12). Furthermore, the calculated diffusion coefficients parallel and perpendicular to the tilt axis are comparable with and lie on either side of the ‘‘average’’ GB self-diffusion values measured on polycrystalline samples.<sup>45</sup> Although it was not our purpose to accurately reproduce experimental data, the observed agreement with such data confirms the reasonable character of our model and simulation techniques.

#### G. Point defect generation/annihilation

The equilibrium concentration of point defects in a GB depends on temperature and other factors such as applied mechanical stresses. If a GB is suddenly heated to a higher temperature, additional point defects will be generated to reach thermodynamic equilibrium at the new temperature. Since each act of defect generation is a thermally activated process, it will take some relaxation time before enough defects have been created to achieve the new equilibrium level. Similarly, if the temperature suddenly drops, it will take some time before the GB reduces the point defect concentration to the new equilibrium level by defect annihilation. In many applications, it is important to know how fast a GB can re-establish a new point defect equilibrium if external conditions suddenly change. For example, processes such as creep, sintering, cavitation, radiation damage and others may critically depend on how effectively GB's can act as sinks or

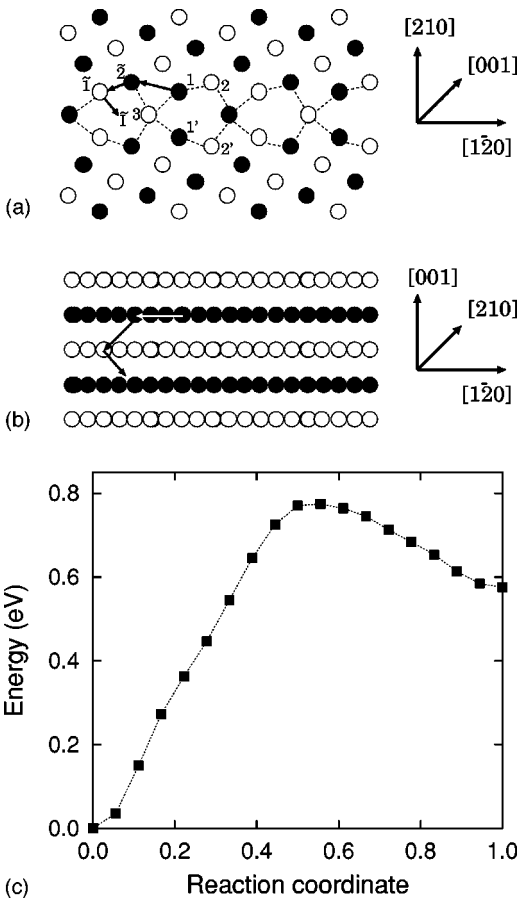


FIG. 13. Formation of a Frenkel pair in the (210)[001] GB. The arrows show displacements of atoms. Two projections of the GB structure are shown: (a) Projection normal to the GB plane. (b) Projection parallel to the GB plane. (c) Energy along the minimum energy path of the pair formation.

sources of point defects. The assessment and prediction of this effectiveness requires a knowledge of atomic mechanisms of point defect generation and annihilation in GB's. Like for GB diffusion, such mechanisms are not well known at present.

The simulation approach introduced in this work for GB diffusion can also be applied for studying point defect generation/annihilation processes. This can be achieved by running basin-constrained MD for a defect-free GB and detecting spontaneous transitions resulting in the appearance of point defects. Since the transitions are reversible, the mechanisms found for defect generation will work for defect annihilation as well. The results obtained on the two  $\Sigma=5$  GB's studied here are briefly discussed below. Our goal here is to illustrate how our method can work for this purpose rather than undertake a comprehensive study of defect generation/annihilation phenomena.

One type of mechanism found by the simulations is the generation of Frenkel pairs (vacancy-interstitial pairs). A Frenkel pair generation process in the (210) GB is illustrated in Fig. 13. The transition has an energy barrier of 0.776 eV. It involves a concerted motion of three atoms (1,  $\tilde{2}$ , and  $\tilde{1}$ ) and results in an interstitial and a vacancy separated by a vector having a [001] component along the tilt axis. Because the defects are well separated, the energy of the pair is close

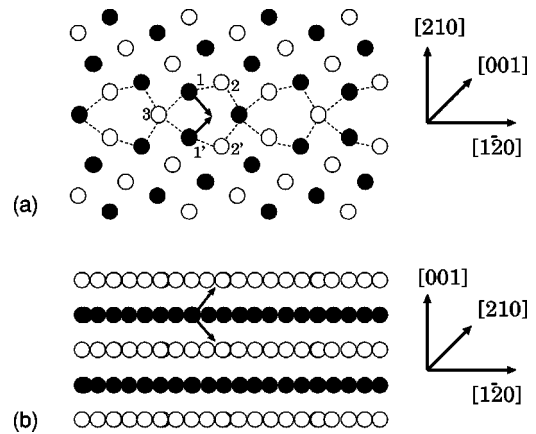


FIG. 14. Formation of an interstitial dumbbell in the (210)[001] GB. The arrows show displacements of atoms. Two projections of the GB structure are shown: (a) Projection normal to the GB plane. (b) Projection parallel to the GB plane.

to the sum of individual defect formation energies. As one would expect, the vacancy is formed at site 1 which offers the lowest vacancy formation energy.

The Frenkel pair formation in GB's is a collective process. At first sight, a Frenkel pair could form by a single-atom jump to a neighboring interstitial site. However, calculations show that this pair would be unstable, in that the atomic relaxations would bring the atom back to its original position. We found that there is a critical separation of the defects at which the pair becomes stable and does not annihilate during the relaxation process. Because this separation is relatively large ( $\sim 6$  Å), a stable pair forms by a collective transition involving displacements of several atoms. As an example, Fig. 13(c) shows the energy along a NEB-calculated minimum-energy path corresponding to the Frenkel pair formation. The fact that there are only two energy minima along the path, corresponding to the initial state and a stable pair, confirms that the three atoms move in a concerted manner. Once a stable Frenkel pair has been created, it may dissociate and the constituent point defects can diffuse along the GB by their own mechanisms. Generation of Frenkel pairs was previously observed by MD simulations in a  $\Sigma=5$  (310)[001] GB in bcc Fe.<sup>3</sup>

Another defect generation mechanism, which we call an interstitial dumbbell formation, is illustrated in Fig. 14 for the (210) GB. In this case, atoms 1 and 1' move simultaneously in opposite directions, each towards the nearest interstitial site  $I$  or  $I^*$ . Alternatively, this process can be viewed as a  $90^\circ$  rotation of the dumbbell formed by atoms 1 and 1' around the  $[1\bar{2}0]$  axis, aligning it parallel to the tilt axis. Once formed, the interstitial dumbbell can annihilate either by a return rotation or by another  $90^\circ$  rotation in the same direction. In the latter case, the two rotations will result in swapping atoms 1 and 1', which provides another diffusion mechanism for tracer or impurity atoms in the GB. The barrier of the interstitial dumbbell formation is 0.757 eV. This mechanism can work in the (310) GB as well, the respective barrier being even slightly lower (0.679 eV). Again, an interstitial dumbbell can dissociate, after which the constituent defects can move independently.

The simulations also revealed other, more complex defect generation mechanisms. For example, the (310) GB can generate pairs of interstitial dumbbells aligned parallel to the tilt axis. Such complex mechanisms involve more atoms moving collectively, and tend to have higher barriers than the mechanisms considered above. We note finally that we only considered defect generation mechanisms in ideal ground-state GB structures. Extended defects, like GB dislocations or steps, serve as point defect sources or sinks as well.

#### H. GB diffusion at high temperatures

Our approach to modeling GB diffusion is based on approximations that are expected to be accurate at relatively low temperatures, for instance at room temperature. This is the relevant temperature regime for many practical materials applications. However, since most radiotracer experiments are carried out at high temperatures, we extended our KMC simulations to that regime, as described above. In this section we discuss the approximations in our approach and address its temperature range of applicability.

A fundamental assumption in our model is that GB diffusion is mediated by noninteracting point defects. This assumption is appropriate when the point defect concentration is relatively low. In the (310) GB, the vacancy occupation probability at any site, estimated from Eq. (1), remains below  $6 \times 10^{-3}$  up to the bulk melting temperature  $T_m = 1357$  K. The interstitial concentration is higher, around 0.1 at  $T_m$ . In the higher-energy (210) GB, the interstitial concentration is low, whereas the vacancy occupation probabilities at sites 1 and 2 are around 0.3 at a temperature of 1000 K. At such high defect concentrations, the assumption of noninteracting defects may be questionable. At temperatures below half the bulk melting point, the point defect occupation probabilities at any site in the two GB's are lower than 0.06; at room temperature they are below  $10^{-4}$ .

Another approximation in our model is that the defect concentrations and transition rates are calculated within the harmonic approximation to atomic vibrations. Foiles<sup>46</sup> has shown that the quasiharmonic approximation underestimates the temperature variation of the formation free energy of a vacancy in Cu (as modeled by an EAM potential). Deviations start to become significant at temperatures roughly around 600 K, when the anharmonicity of the potential energy surface becomes important. Regarding the effect of anharmonicity on the transition rate constants, simulations<sup>24</sup> of atomic transitions in metals (modeled by EAM potentials) have shown that one should expect the rate constant predicted from harmonic TST to deviate by up to a factor of 2–4 from the rate constant calculated directly with MD, at high temperatures (700–1000 K). The deviation is smaller at lower temperatures.

It should also be stressed that our KMC simulations were based on a small subset of atomic transitions. This subset consisted of the low-barrier processes that dominate diffusion at low temperatures, but as the temperature is raised, processes with higher barriers could also contribute to diffusion. This could lead to an upwards curvature in the Arrhenius plots of diffusion coefficients. We preferred to keep the KMC model simple and the analysis transparent, rather than include more transitions in the model.

The observation that some defect concentrations become very high as the temperature increases raises the concern that the GB might lose its atomic order at some temperature below the bulk melting point. Such disorder might invalidate not only our results but also the concept of point defects itself. To study the GB structure at high temperatures, we carried out Metropolis Monte Carlo (MC) simulations at temperatures of 1000 K and above. We found that both GB's maintained their ground-state structure and long-range order at  $T = 1000$  K. The (210) GB showed more significant distortions of the initial structure than did the (310) GB. This is understandable in view of greater atomic relaxations around vacancies in the (210) GB (cf. Fig. 4). The initial structure of the (210) GB could still be recognized at temperatures up to about 1100 K, and the structure of the (310) GB up to even higher temperatures. However, at temperatures above 1200 K the distortions became so large that a conclusive comparison could not be made. We note that our MC simulations did not reveal any first-order structural phase transformations in the GB's. Namely, when we “quenched” the high-temperature ( $T > 1200$  K) states by static relaxation we always obtained the ground-state GB structure containing a few point defects.

Recently, Wolf and co-workers<sup>7</sup> found from MD simulations that at high temperatures, some high-energy GB's in Pd underwent a transition to a partially disordered, liquidlike structure. They observed a corresponding change in the diffusion behavior from solidlike to liquidlike. Our study deals with the solidlike regime that prevails at low to moderate temperatures and investigations of higher temperatures are beyond the scope of this paper.

#### IV. CONCLUSION

In this paper we investigated atomic diffusion mechanisms in GB's using a computer simulation approach that combines (i) basin-constrained MD with an automated location of transition states, (ii) molecular statics in conjunction with harmonic calculations of atomic vibrations, and (iii) KMC simulations. Our key assumption is that GB diffusion takes place by thermally activated motion of independent point defects via local transitions. Our approach has the following advantages over previous studies in this area:

1. The atomic mechanisms of GB diffusion are not postulated but rather inferred from MD simulations. This allows us to study mechanisms that could hardly be guessed *a priori*.

2. Our simulations are not limited to single-atom jumps. By using the NEB method<sup>15</sup> we can investigate more complex, “collective” transitions involving a concerted motion of several atoms.

3. The point defect formation entropies and attempt frequencies are calculated directly within the harmonic approximation to lattice vibrations and transition state theory.<sup>29</sup> In that way we avoid using empirical correlations between defect energies and entropies as it was done in previous studies.<sup>6,8,13,14</sup> In fact, our results summarized in Tables II and III indicate that such correlations do not work for point defects in GB's with any reasonable accuracy.

4. We apply a generalized KMC scheme that allows for both vacancy and interstitial-related mechanisms and includes collective transitions.

We have applied this approach to study diffusion in  $\Sigma = 5$  [001] (210) and (310) symmetric tilt GB's in Cu. Although the  $\Sigma = 5$  GB's studied here represent only the simplest type of high-angle GB's showing significantly enhanced diffusion rates over the perfect lattice, many of our conclusions appear to be rather general and may apply to other types of GB's as well. Our conclusions can be summarized as follows.

GB's are able to support vacancies and interstitials. Interstitials in GB's can have significantly lower formation energies than in the perfect lattice, and thus can play an important role in GB diffusion. Vacancy formation energies vary significantly from site to site, being lower than in the lattice at some GB sites but higher than in the lattice at other GB sites. Two important effects associated with vacancy formation in GB's have been found in this work. First, a vacancy can delocalize in a GB by giving rise to local relaxations so strong that the associated free volume can no longer be assigned to a certain site. An example is offered by site 1 in the (210) GB [Fig. 4(a)]. Second, certain GB sites do not support vacancies at all. If created by removing an atom from such a site, the vacancy is unstable and gets filled by a nearby atom during the relaxation process. For example, site 6 in the (310) GB does not support a stable vacancy [Fig. 2(b)]. It should be admitted, however, that most GB sites do support stable localized vacancies (see example in Fig. 5).

Vacancies can move along GB's by simple vacancy-atom exchanges, as they do in the lattice. Although this appears to be the most common vacancy-related mechanism of GB diffusion, vacancies can also move by collective transitions ("long jumps") involving two or more atoms. The result of a long vacancy jump is the same as for a sequence of two or more single-atom jumps, but the difference is that the atoms involved in a long jump move simultaneously in a concerted manner. The easiest long vacancy jump found in this work is the transition  $1 \rightarrow 6 \rightarrow \tilde{4}$  in the (310) GB [Fig. 6(b)], where the vacancy moves via an intermediate, unstable vacancy site. This example demonstrates that long vacancy jumps may have barriers comparable with those for single-atom jumps, and that long jumps can be of critical importance for GB diffusion. In particular, the  $1 \rightarrow 6 \rightarrow \tilde{4}$  transition is the bottleneck for vacancy diffusion perpendicular to the tilt axis in the (310) GB. We expect that other GB structures may show a larger variety of collective transitions involving vacancies.

Direct interstitial jumps turn out to be relatively unfavorable for the investigated GB's. Instead, interstitials move by the interstitialcy mechanism that again involves collective displacements of at least two atoms (Figs. 7 and 8). Another interesting finding is the observation of ring processes involving up to six atoms [Figs. 8(c) and 9]. Although complex transitions involving groups of atoms tend to have higher activation barriers, we believe that some of them can play a role at high temperatures. It is also possible that such types

of long-range mechanisms could be important in other materials or GB structures.

We have carried out KMC simulations of GB diffusion by different mechanisms in a wide temperature range. The simulations revealed that GB diffusion can be dominated by either vacancy or interstitial-related mechanisms depending on the GB structure. In particular, regardless of the diffusion direction or temperature, diffusion in the (210) GB is dominated by the vacancy mechanism while diffusion in the (310) GB is dominated by the interstitialcy mechanism. The diffusion coefficients obtained by KMC simulations were found to follow an Arrhenius law in the temperature range of calculations (Fig. 10). In many cases the apparent activation energy of GB diffusion can be traced back to a specific transition or a set of transitions with nearly identical partial activation energies (cf. Tables III and V).

The KMC simulations also reveal interesting effects associated with atomic jump correlations in GB's. For example, correlation factors can be significantly temperature-dependent with very small values at low temperatures (Fig. 11). The small correlation factors are caused by a trapping effect arising from multiple back-and-forth jumps between sites separated by a low barrier. While the trapping effect was earlier observed for GB diffusion by the vacancy mechanism,<sup>10</sup> in the present case it is associated with diffusion by the interstitialcy mechanism.

The simulation approach introduced in this work for GB diffusion has a larger area of applications. As an illustration, we have used it to study atomic mechanisms of point defect generation/annihilation in GB's. At least for the GB's we investigated, the easiest mechanisms are the formation/annihilation of Frenkel pairs and interstitial dumbbells. Both mechanisms, illustrated in Figs. 13 and 14, again involve a collective motion of several atoms.

The approximations in our approach are most accurate at low to moderate temperatures. At high temperatures, our results will be less accurate for the following reasons: (i) interactions between defects may start to play a role as the defect concentration increases, (ii) anharmonicity may affect the defect concentrations and transition rate constants, and (iii) high-barrier transitions not included in the present KMC model may contribute to diffusion. The GB's studied here maintained their ordered structure until at least 1000 K. At temperatures above 1200 K, distortions of the GB structure induced by thermal motion of atoms are so strong that the picture of single point defects in an ordered GB may not be justified. GB diffusion at such temperatures may occur by significantly different atomic mechanisms, perhaps liquidlike mechanisms as suggested in Ref. 7.

#### ACKNOWLEDGMENTS

This work was supported by the U.S. Department of Energy under Contracts No. W-7405-ENG-36 (M.R.S. and A.F.V.) and DE-FG02-99ER45769 (Y.M.).

- <sup>1</sup>I. Kaur, Y. Mishin, and W. Gust, *Fundamentals of Grain and Interphase Boundary Diffusion* (Wiley, Chichester, 1995).
- <sup>2</sup>Y. Mishin, Chr. Herzig, J. Bernardini, and W. Gust, *Int. Mater. Rev.* **42**, 155 (1997).
- <sup>3</sup>T. Kwok, P. S. Ho, and S. Yip, *Phys. Rev. B* **29**, 5354 (1984).
- <sup>4</sup>T. Kwok, P. S. Ho, and S. Yip, *Phys. Rev. B* **29**, 5363 (1984).
- <sup>5</sup>S. J. Plimpton and E. D. Wolf, *Phys. Rev. B* **41**, 2712 (1990).
- <sup>6</sup>C. L. Liu and S. J. Plimpton, *Phys. Rev. B* **51**, 4523 (1995).
- <sup>7</sup>P. Kębliński, D. Wolf, S. R. Phillpot, and H. Gleiter, *Philos. Mag. A* **79**, 2735 (1999).
- <sup>8</sup>Q. Ma, C. L. Liu, J. B. Adams, and R. W. Balluffi, *Acta Metall. Mater.* **41**, 143 (1993).
- <sup>9</sup>Q. Ma and R. W. Balluffi, *Acta Metall. Mater.* **42**, 1 (1994).
- <sup>10</sup>Y. Mishin, *Philos. Mag. A* **72**, 1589 (1995).
- <sup>11</sup>Y. Mishin and Chr. Herzig, *Philos. Mag. A* **71**, 641 (1995).
- <sup>12</sup>Y. Mishin, *Defect Diffus. Forum* **143-147**, 1357 (1997).
- <sup>13</sup>M. Nomura and J. B. Adams, *J. Mater. Res.* **10**, 2916 (1995).
- <sup>14</sup>M. Nomura and J. B. Adams, *J. Mater. Res.* **7**, 3202 (1992).
- <sup>15</sup>H. Jónsson, G. Mills, and K. W. Jacobsen, in *Classical and Quantum Dynamics in Condensed Phase Simulations*, edited by B. J. Berne, G. Ciccotti, and D. F. Coker (World Scientific, Singapore, 1998).
- <sup>16</sup>Q. Ma and R. W. Balluffi, *Acta Metall. Mater.* **41**, 133 (1993).
- <sup>17</sup>J. Sommer, Chr. Herzig, T. Muschik, and W. Gust, *Acta Metall. Mater.* **43**, 1099 (1995).
- <sup>18</sup>E. Budke, T. Surholt, S. I. Prokofjev, L. S. Shvindlerman, and Chr. Herzig, *Acta Mater.* **47**, 385 (1999).
- <sup>19</sup>C. K. Hu and J. M. E. Harper, *Mater. Chem. Phys.* **52**, 5 (1998).
- <sup>20</sup>A. F. Voter, *Phys. Rev. B* **57**, R13 985 (1998).
- <sup>21</sup>A. F. Voter, in *Intermetallic Compounds*, edited by J. H. Westbrook and R. L. Fleischer (John Wiley and Sons, New York, 1994), Vol. 1.
- <sup>22</sup>A. F. Voter, Los Alamos Unclassified Technical Report # LA-UR 93-3901, 1993 (unpublished).
- <sup>23</sup>A. P. Sutton and R. W. Balluffi, *Interfaces in Crystalline Materials* (Clarendon Press, Oxford, 1995).
- <sup>24</sup>M. R. Sørensen and A. F. Voter, *J. Chem. Phys.* **112**, 9599 (2000).
- <sup>25</sup>M. R. Sørensen, K. W. Jacobsen, and H. Jónsson, *Phys. Rev. Lett.* **77**, 5067 (1996).
- <sup>26</sup>D. J. Wales and J. Uppenbrink, *Phys. Rev. B* **50**, 12 342 (1994).
- <sup>27</sup>L. J. Munro and D. J. Wales, *Phys. Rev. B* **59**, 3969 (1999).
- <sup>28</sup>G. Henkelman and H. Jónsson, *J. Chem. Phys.* **111**, 7010 (1999).
- <sup>29</sup>G. H. Vineyard, *J. Phys. Chem. Solids* **3**, 121 (1957).
- <sup>30</sup>G. E. Murch and I. V. Belova, in *Diffusion Mechanisms in Crystalline Materials*, edited by Y. Mishin, G. Vogl, N. Cowern, R. Catlow, and D. Farkas, MRS Symposium Proceedings No. 527 (Materials Research Society, Warrendale, Pennsylvania, 1998), p. 135.
- <sup>31</sup>The actual number of atoms in the block is  $nN_s \pm 1$  with a + sign for an interstitial and a - sign for a vacancy.
- <sup>32</sup>J. R. Manning, *Diffusion Kinetics for Atoms in Crystals* (Van Nostrand, Princeton, New Jersey, 1968).
- <sup>33</sup>P. Zhao and Y. Shimomura, *Comput. Mater. Sci.* **14**, 84 (1999).
- <sup>34</sup>M. S. Daw and M. I. Baskes, *Phys. Rev. B* **29**, 6443 (1984).
- <sup>35</sup>R. A. Johnson and E. Brown, *Phys. Rev.* **127**, 446 (1962).
- <sup>36</sup>N. Tajima, O. Takai, Y. Kogure, and M. Doyama, *Comput. Mater. Sci.* **14**, 152 (1999).
- <sup>37</sup>R. W. Siegel, *J. Nucl. Mater.* **69-70**, 117 (1978).
- <sup>38</sup>R. W. Balluffi, *J. Nucl. Mater.* **69-70**, 240 (1978).
- <sup>39</sup>F. W. Young, *J. Nucl. Mater.* **69-70**, 310 (1978).
- <sup>40</sup>J. Philibert, *Atom Movements—Diffusion and Mass Transport in Solids* (Les Editions de Physique, Les Ulis, 1991).
- <sup>41</sup>*Diffusion in Solid Metals and Alloys*, edited by H. Mehrer, Landolt-Börnstein, New Series, Group III, Vol. 26 (Springer, Berlin, 1990).
- <sup>42</sup>K. Maier, *Phys. Status Solidi A* **44**, 567 (1977).
- <sup>43</sup>C. Zener, in *Imperfections in Nearly Perfect Crystals*, edited by R. Maurer, W. Shockley, J. H. Holloman, and F. Seitz (Wiley, New York, 1952), p. 289.
- <sup>44</sup>A. Seeger, *Defect Diffus. Forum* **95-98**, 147 (1993).
- <sup>45</sup>T. Surholt and Chr. Herzig, *Acta Mater.* **45**, 3817 (1997).
- <sup>46</sup>S. M. Foiles, *Phys. Rev. B* **49**, 14 930 (1994).